



A Journal of the Gesellschaft Deutscher Chemiker

# Angewandte Chemie

GDCh

International Edition

www.angewandte.org

## Accepted Article

**Title:** A Strategy for Construction of a Nanoporous Highly Crystalline Hexagonal Boron Nitride from an Amorphous Precursor

**Authors:** Hao Chen, Zhenzhen Yang, Zihao Zhang, Zitao Chen, Miaofang Chi, Song Wang, Jie Fu, and Sheng Dai

This manuscript has been accepted after peer review and appears as an Accepted Article online prior to editing, proofing, and formal publication of the final Version of Record (VoR). This work is currently citable by using the Digital Object Identifier (DOI) given below. The VoR will be published online in Early View as soon as possible and may be different to this Accepted Article as a result of editing. Readers should obtain the VoR from the journal website shown below when it is published to ensure accuracy of information. The authors are responsible for the content of this Accepted Article.

**To be cited as:** *Angew. Chem. Int. Ed.* 10.1002/anie.201904996  
*Angew. Chem.* 10.1002/ange.201904996

**Link to VoR:** <http://dx.doi.org/10.1002/anie.201904996>  
<http://dx.doi.org/10.1002/ange.201904996>

## COMMUNICATION

# A Strategy for Construction of a Nanoporous Highly Crystalline Hexagonal Boron Nitride from an Amorphous Precursor

Hao Chen, Zhenzhen Yang\*, Zihao Zhang, Zitao Chen, Miaofang Chi, Song Wang, Jie Fu\* and Sheng Dai\*

**Abstract:** Hexagonal boron nitride (h-BN) is regarded as a graphene analogue and exhibits important characteristics and vast application potentials. However, discovering a facile methodology for the preparation of nanoporous crystalline h-BN nanosheets (h-BNNS) is still a challenge. Herein, a novel and simple protocol for the conversion of amorphous h-BN precursors to highly crystalline h-BNNS was achieved through a successive dissolution-precipitation/crystallization process in the presence of magnesium. The fabricated h-BNNS exhibited high crystallinity and high porosity with a surface area of 347 m<sup>2</sup> g<sup>-1</sup>, high purity, and enhanced thermal stability. Improved catalytic performance of crystalline h-BNNS was evidenced by its much higher catalytic efficiency in the dehydrogenation of dodecahydro-N-ethylcarbazole, compared with its amorphous h-BN precursor, as well as other precious metal loaded heterogeneous catalysts. This work provides new insight into the fabrication of nanoporous crystalline h-BNNS, expanding its application in the field of energy storage and transformation.

Two-dimensional (2D) nanomaterials have been the subject of much research since the discovery of mechanically exfoliated graphene with extraordinary physical and chemical properties.<sup>[1-5]</sup> Hexagonal boron nitride (h-BN) has a layered honeycomb-like structure similar to that of graphite, consisting of alternating B and N atoms. A single-layer h-BN nanosheet (h-BNNS) can be regarded as a graphene analogue, which is commonly known as the "white graphene". h-BN structures are characterized by their excellent thermal and chemical stability, and unique electronic and optical properties, which are widely applied in the field of energy storage and transformation.<sup>[2, 6, 7]</sup> Generally, their properties/functionality can vary tremendously depending on their

different structural characteristics, such as size, surface area, thickness, crystal phase, defects, vacancies, etc.<sup>[2, 8-10]</sup>

To date, Hermans et al. reported that bulk h-BN and boron nitride nanotubes (BNNT) exhibited unique and highly efficient catalytic properties for the oxidative dehydrogenation of propane, resulting in great selectivity to olefins (79% propene and 12% ethene at 14% propane conversion).<sup>[11, 12]</sup> Although both bulk h-BN and BNNT exhibited analogous product distributions, BNNT showed a rate of propane consumption more than one order of magnitude higher than that of h-BN, partially because of the higher surface area of BNNT (97 m<sup>2</sup> g<sup>-1</sup>) relative to bulk h-BN (16 m<sup>2</sup> g<sup>-1</sup>), and thus a superior mass transfer effect during the catalytic process. The thickness of the h-BN materials (bulk vs. few layered) also had a significant effect on their properties. Generally, few layered h-BNNS are preferred, which are mostly prepared via either a solid-phase mechanical method<sup>[13]</sup> or liquid-phase exfoliation.<sup>[14, 15]</sup> Our group previously presented an efficient strategy for the scalable synthesis of few-layered h-BNNS using a gas exfoliation of bulk h-BN in liquid N<sub>2</sub>.<sup>[16]</sup> However, the final few-layered h-BNNS obtained through these approaches often suffer from low surface areas or amorphous/low crystalline structures.<sup>[15, 17]</sup> Compared with amorphous materials, their highly crystalline counterparts have ordered structures and fewer defects, thus leading to enhanced performance in optoelectronics and catalysis,<sup>[18]</sup> as shown by the significant development of crystalline metal-organic framework (MOF) nanosheets,<sup>[19]</sup> and 2D covalent organic frameworks (COFs).<sup>[20]</sup> In addition, the high crystallinity makes their structures easier to be determined by using powder X-ray diffraction (PXRD) and high-resolution transmission electron microscopy (HR-TEM). Up to now, the lack of a controlled synthesis of quality h-BN samples largely prevented the full potential of h-BN nanostructures from being realized. Therefore, the development of novel and simple synthetic methodologies for the fabrication of crystalline few-layered h-BNNS with a high surface area would propel further advancement in this field, despite still being a challenging task.

We hypothesized whether it was possible to construct highly crystalline and porous h-BNNS from amorphous h-BN. Recently, this protocol was utilized in the conversion of amorphous covalent organic polymers (COPs) to COFs of high crystallinity and porosity by replacing the linkers.<sup>[21]</sup> Herein, a novel strategy was developed for the successful transformation of amorphous bulk h-BN to h-BNNS with high crystallinity and porosity, which was fully characterized by powder X-ray diffraction (PXRD), microscopy and N<sub>2</sub> adsorption/desorption isotherms. The essence of this strategy lies in the successive dissolution-precipitation/crystallization of amorphous h-BN precursor in the presence of magnesium (Mg) (Figure 1A). The produced crystalline h-BNNS consisted primarily of thin layers in a high mass yield of 88%. The N<sub>2</sub> sorption and desorption isotherm exhibited a surface area of 347 m<sup>2</sup> g<sup>-1</sup> and total pore volume of 0.41 cm<sup>3</sup> g<sup>-1</sup> with a pore size distribution dominated by mesopores. The

- [a] Dr. H. Chen, Dr. J. Fu, Z. Zhang  
Key Laboratory of Biomass Chemical Engineering of Ministry of Education, College of Chemical and Biological Engineering Zhejiang University, Hangzhou, 310027, China.  
E-mail: jiefu@zju.edu.cn
- [b] Dr. Z. Yang, Dr. H. Chen, Dr. S. Dai  
Chemical Sciences Division, Oak Ridge National Laboratory, Oak Ridge, TN 37831, United States.  
E-mail: dais@ornl.gov
- [c] Dr. Z. Yang, Dr. H. Chen, Dr. S. Dai  
Department of Chemistry, The University of Tennessee, Knoxville, TN, 37996, United States.  
E-mail: zyang17@utk.edu
- [d] S. Wang  
Department of Chemistry, University of California, Riverside, California 92521, United States.
- [e] Z. Chen, M. Chi  
Center for Nanophase Materials Sciences, Oak Ridge National Laboratory, Oak Ridge, Tennessee 37831, United States

Supporting information for this article is given via a link at the end of the document.

## COMMUNICATION

enhanced structure patterns and thermal stability render it as an efficient catalyst in the dehydrogenation of dodecahydro-N-ethylcarbazole, exhibiting a much higher catalytic efficiency compared with the amorphous h-BN precursor, as well as other precious metal loaded heterogeneous catalysts reported previously.

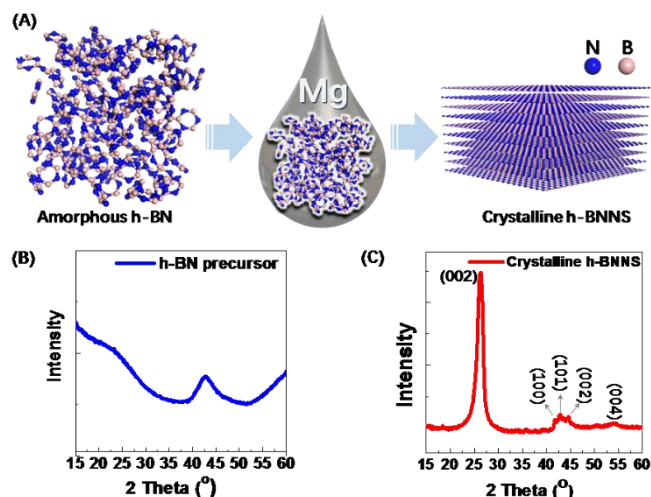


**Figure 1.** (A) The general strategy used in this work for the conversion of amorphous h-BN to crystalline h-BNNS. (B) PXRD patterns of the bulk h-BN precursor and (C) the obtained crystalline h-BNNS.

The amorphous h-BN precursor was first synthesized according to a previously reported procedure with boric acid and urea (molar ratio 1:24) as the reactants, which was calcined at 900 °C for 2 h under N<sub>2</sub> atmosphere (for details, see Supporting Information).<sup>[22]</sup> The PXRD pattern of the bulk h-BN samples (Figure 1B) showed only one broad tiny diffraction peak at 2θ = 42.5 degrees, which was indexed at (100) planes of h-BN, and no obvious diffraction (002) peak at 2θ = 27.0 degree was observed, indicating almost no crystallinity of the h-BN precursor. It is well known that catalysts such as metal elements, oxides, and salts, can significantly lower the graphitization temperature of soft carbons and enable the graphitization of hard carbons.<sup>[23, 24]</sup> Our group has reported a simple electrochemical route for the graphitization of amorphous carbons through cathodic polarization in molten CaCl<sub>2</sub>, and the resultant nanostructured graphite exhibited good performance as a superior cathode material for batteries.<sup>[25]</sup> In this work, a crystallization strategy was adopted for the transformation of h-BN material in the presence of molten metals. Magnesium was selected as the reagent used to treat the amorphous h-BN precursor, considering its appropriate melting point (650 °C) and good performance in the fabrication of crystalline graphite powder from renewable hard carbon precursors.<sup>[26]</sup> The recrystallization process is illustrated in Figure 1A. The h-BN precursor was first mixed with Mg powder, and then the mixture was sealed in stainless-steel tubes and treated at 900 °C under N<sub>2</sub> atmosphere (for details, see Supporting Information). After removing the Mg by washing, crystalline h-BN was obtained with a yield of 88 % by weight. The atomically precise periodic architecture of the obtained h-BN was investigated by PXRD, and these data match well with a typical hexagonal structure of h-BN (JCPDS card no. 01-073-2095).<sup>[2]</sup> A strong diffraction (002) peak at 2θ = 26.41 degrees corresponds to the

interplanar distance of 3.5 Å. Other relatively weaker diffraction peaks at 2θ = 41.88, 42.93, 44.46 and 54.08 degrees are assigned to (100), (101), (002), and (004) crystal planes, respectively, suggesting the formation of highly crystalline h-BN with an extended/ordered stacking in the c direction.<sup>[27]</sup> These results confirm that this method can effectively transform the bulk amorphous precursor into highly crystalline h-BN.

In order to illustrate the morphological change after treatment with Mg, scanning electron microscopy (SEM) images of the parent bulk amorphous h-BN and obtained crystalline h-BN are shown in Figure 2A and 2B. The bulky h-BN precursor is mainly composed of big blocks containing randomly packed layers of large lateral size and thickness (>3.5 μm). Comparatively, the crystalline h-BN demonstrates a petaloid flakes morphology of much smaller lateral size (≈200 nm) with a thickness of about 12.9 nm. Meanwhile, transmission electron microscopy (TEM) images of the h-BN precursor and the crystalline h-BN also exhibit distinct differences. Figure 2D shows that the crystalline h-BN has a transparent and overlapped flat structure, whereas the parent amorphous h-BN has a bulky and opaque structure with numerous wrinkles and crimps, as shown in Figure 2C, which provides clear evidence that the bulky h-BN precursor is reorganized into sheet-like patterns. In the region of higher contrast in Figure 2D, the curved edge can be seen and the thickness of one sheet-like structure is found to be approximately 13.1 nm, consistent with the thickness measured in the SEM image. Figure 2E and 2F are an enlarged selective area of Figure 2C and 2D, respectively. HR-TEM images of the parent h-BN precursor showed no lattice fringes, while HR-TEM images of the crystalline h-BN exhibited one set of lattice fringes with a spacing of 0.35 nm, corresponding to the (002) plane of the six-fold symmetry of h-BN. Given that the thickness of a single-layered h-BN is about 0.4-0.5 nm,<sup>[28]</sup> the observation suggests that the as-prepared crystalline h-BNNS consists about 15-20 atomic layers in each sheet. The electron diffraction pattern suggests the amorphous structure of the h-BN precursor (Figure 2G) and the typical six-fold symmetry structure of the obtained crystalline h-BNNS (Figure 2H and 2I).

The Fourier transform infrared (FTIR) spectra of the raw h-BN material and the crystalline h-BNNS are shown in Figure S1. In the original h-BN, two characteristic peaks are observed at about 1323.5 cm<sup>-1</sup> and 798.1 cm<sup>-1</sup>, which are attributed to in-plane B-N stretching vibrations and out of plane bending, respectively. After recrystallization, the two peaks showed a slight blueshift to 1341.7 cm<sup>-1</sup> and 807.7 cm<sup>-1</sup>, respectively, owing to the ordered pattern and connection of the hexagonal structure within the h-BN framework, as well as perhaps a composition change after treatment by Mg. Further X-ray photoelectron spectroscopy (XPS) analysis was conducted to gain more information on the surface structure change of the h-BN (Figure S2). In the h-BN precursor, the main peaks with a binding energy (BE) of 190.8 eV in the B1s and 398.5 eV in the N1s correspond to B-N bonds. In addition, the B-O bond with BE=192.3 eV and N-C bond with BE=400.1 eV are also exhibited within the h-BN framework, and are in close agreement with the reported data.<sup>[13]</sup> Comparatively, the crystalline h-BNNS after treatment by Mg powder only showed a signal of B-N bonds with BE=190.3 eV in B1s and BE=397.9 eV in N1s, indicating that most of the residual carbon and oxygen elements from the starting materials were further removed during the heating process through combination with Mg, resulting in high-purity h-BN. The removal of oxygen atoms during the recrystallization process is also evidenced by the magic angle

## COMMUNICATION

spinning (MAS)  $^{11}\text{B}$  solid-state NMR spectroscopy (Figure S3). In the  $^{11}\text{B}$  spectra of the h-BN precursor, an obvious signal for  $\text{BO}_3$  is shown at  $-0.72$  ppm, which disappears in the crystalline h-BNNS. Both the h-BN precursor and the crystalline h-BNNS exhibited  $^{11}\text{B}$  signals at 10.2 ppm and 26.1 ppm, which is attributed to the  $\text{BN}_3$  structure.<sup>[29]</sup> Although h-BN generally exhibited high thermal stability considering its fabrication process performing at high temperature under  $\text{N}_2$ , inevitable residual carbon and oxygen elements within the backbone will lead to decreased thermal stability under air. Thermogravimetric analysis (TGA) of the h-BN precursor showed a weight loss beginning at  $260^\circ\text{C}$  under air (Figure S4), probably caused by the loss of carbon atoms, with the weight loss reaching  $\sim 30$  wt% up to  $800^\circ\text{C}$ . A further increase in temperature led to a slight increase in the sample weight due to the combination of boron in  $\text{BN}_2$  or  $\text{BN}$  units with oxygen atoms in the air. Comparatively, only a slight weight loss in the crystalline h-BNNS was observed from  $520^\circ\text{C}$  ( $<10$  wt%), demonstrating its enhanced thermal stability.

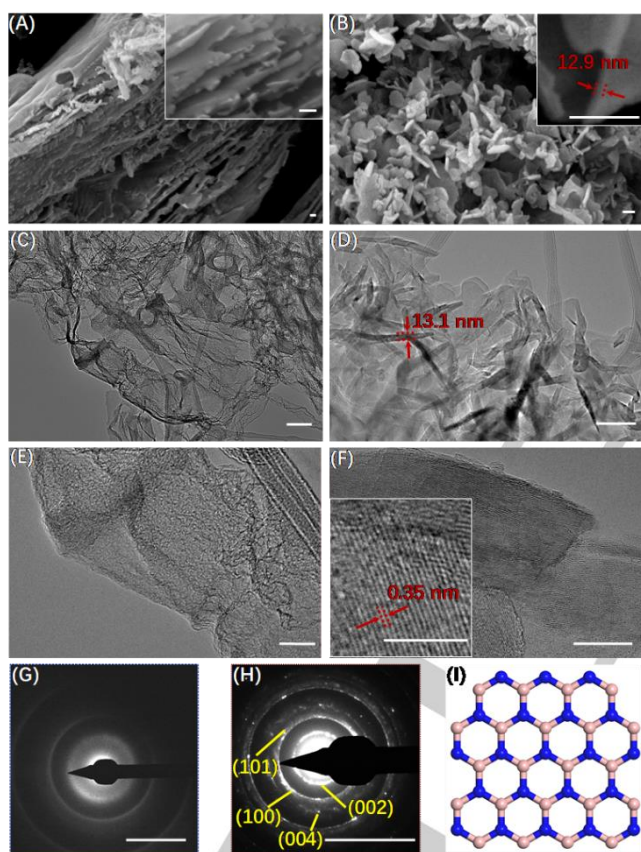


**Figure 2.** (A) SEM image of the bulk h-BN precursor and (B) crystalline h-BNNS. (C, E) (HR)-TEM image of h-BN precursor and (D, F) crystalline h-BNNS. (G) Electron diffraction pattern of h-BN precursor and (H) crystalline h-BNNS. (I) Hexagonal structure of h-BN. The inset images magnify selected regions. Scale bar 100 nm for (A–D), 20 nm for (E, F), 5 1/nm for (G) and 10 1/nm for (H).

The permanent porosity of crystalline h-BNNS was measured by  $\text{N}_2$  adsorption/desorption analysis at 77 K (Figure S5). The  $\text{N}_2$  sorption isotherms exhibited combined features of type I and type IV with two evident step steps in the regions of  $P/P_0=0-0.01$  and  $0.80-0.98$ ,

suggesting the coexistence of micro- and mesopores. Based on the calculated result of the non-local density functional theory method (NLDFT), it was clear that micropores around 1.06–1.92 nm in size and mesopores with pore diameters in the range of 2–13.5 nm were present. The Brunauer–Emmett–Teller (BET) surface area of the crystalline h-BN was estimated to be  $347\text{ m}^2\text{ g}^{-1}$ , owing to the high surface area of the amorphous precursor (Figure S5 D–F), with a total pore volume of  $0.41\text{ m}^3\text{ g}^{-1}$ . Notably, mesopores played a dominant role in the pore structure, contributing  $\sim 99\%$  of the total pore volume ( $V_{\text{micro}}=0.0085\text{ cm}^3\text{ g}^{-1}$ , calculated using the  $t$ -plot method). For catalytic or adsorptive materials, this high surface area can enhance their reactivity due to an improved mass transfer effect. The result further suggested that the method developed in this work is highly efficient in generating few-layered nanoporous crystalline h-BNNS of high purity, high surface area and high thermal stability.

Encouraged by the above results, we conducted time-dependent experiments to gain better insight into the transformation of amorphous h-BN to crystalline h-BN. As shown in Figure 3A, PXRD results of the materials obtained at different calcination times indicated that the long-range ordering of h-BN already occurred when the reaction time reached 40 min, and the crystallinity of h-BNNS gradually increased from 20 min to 60 min. Heat treatment temperatures are also very critical to the recrystallization of the h-BN precursor. As mentioned above, crystalline h-BNNS can be obtained at a calcination temperature of  $900^\circ\text{C}$ . Under otherwise identical treatment conditions, the h-BN samples obtained at calcination temperatures of  $800^\circ\text{C}$  and  $1000^\circ\text{C}$  led to amorphous materials, as shown by the PXRD patterns (Figure 3B). The SEM images showed that h-BN obtained at  $800^\circ\text{C}$  were still big blocks with thick layers (Figure S6), somewhat like the h-BN precursor, while h-BN obtained at  $1000^\circ\text{C}$  became bulky particles. This indicated that the appropriate temperature is needed for the solubilization of h-BN in molten Mg, but too high a temperature led to the shrinkage of the h-BN skeleton. The PXRD results also showed that a short reaction time (20 min) or low heating temperature led to a small amount of carbon nitride (JCPDS card no. 50-0664) formation within the obtained h-BN samples. As previously reported, dissolution-precipitation mechanism and formation-decomposition of carbide intermediate mechanism have been proposed to explain the graphitization process in the presence of metal catalysts.<sup>[26, 30]</sup> Considering the the high thermal stability of h-BN (up to  $2800^\circ\text{C}$ ) under  $\text{N}_2$ ,<sup>[31]</sup> the recrystallization process of h-BN in this work was estimated to proceed through a dissolution-precipitation mechanism.

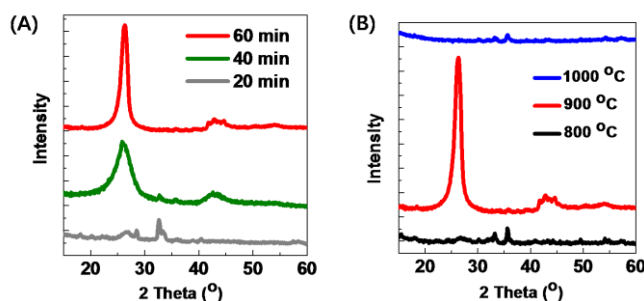


**Figure 3.** PXRD patterns of h-BN obtained at (A) different calcination time and (B) different heating temperature.

## COMMUNICATION

Handling hydrogen in chemically bound form as liquid organic hydrogen carriers (LOHCs) supports concept that a future hydrogen economy may work without the need to handle large amounts of elemental hydrogen.<sup>[32-34]</sup> But the realization of this future economy relies on the development of a highly efficient catalytic system for the reversibility and high selectivity of LOHC,<sup>[35]</sup> especially the N-ethylcarbazole (NEC) and dodecahydro-N-ethylcarbazole (12H-NEC) cycle systems.<sup>[36]</sup> However, even after decades of research, the unsatisfactory performance obtained using high doses of precious-metal dehydrogenation catalysts and the required high reaction temperatures has proven to be a bottleneck (Table S1).<sup>[34]</sup> Considering the highly efficient catalytic activity of h-BN in oxidative dehydrogenation of propane (ODHP) for olefin production,<sup>[11, 12, 37, 38]</sup> we envisioned that the crystalline nanoporous h-BNNS obtained in this study could act as an efficient metal-free catalyst for the dehydrogenation of 12H-NEC. Indeed, taking NEC-12H as a model substrate (Figure 4), a 74% yield of NEC was obtained using the as-prepared crystalline h-BNNS as the catalyst at a low reaction temperature (120 °C). Notably, this yield is much higher than that obtained by the bulk amorphous h-BN (NEC yield: 40%), commercialized h-BN (NEC yield: 10%) as well as Pd/C (NEC yield: 5.2%) under the same conditions. The enhanced catalytic activity of crystalline h-BNNS is also observed in the dehydrogenation of dodecahydro-N-propylcarbazole (12H-NPC) with a yield of N-propylcarbazole (NPC) as 63% (crystalline h-BNNS) and 36% (amorphous h-BN). Notably, the catalytic efficiency of h-BNNS is much higher than that of Pd-, Pt-, Ru-loaded heterogeneous catalysts previously reported (Table S1). According to the previously reported literatures,<sup>[11, 39]</sup> the dehydrogenation process of 12H-NEC is proposed to include the adsorption of 12H-NEC on the B sites, cleavage of the C-H bond and formation of H<sub>2</sub> gas. We proposed that the synergistic effect of the nanoporous structure (beneficial to mass transport) and highly ordered crystalline pattern of h-BNNS (exposure of more B sites) plays crucial role in achieving this superior dehydrogenation performance.

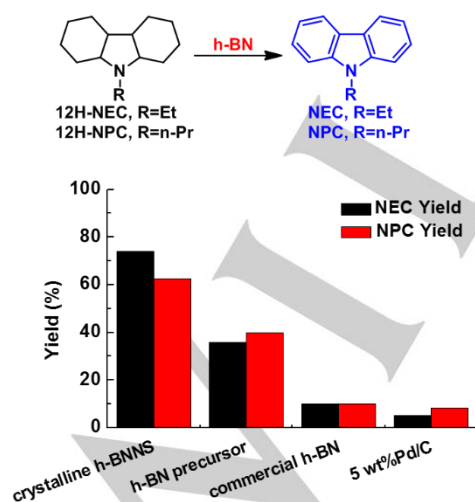


**Figure 4.** Comparison of the catalytic efficiency of various catalysts including the crystalline h-BNNS for the dehydrogenation of 12H-NEC.

In conclusion, we have developed a novel strategy used to construct highly crystalline nanoporous h-BNNS through the transformation of amorphous h-BN precursors in the presence of Mg. The as-prepared h-BNNS are characterized by high crystallinity, high purity, high porosity and high thermal stability. These desirable structural patterns and properties render enhanced catalytic efficiency and potential application of h-BNNS in the dehydrogenation of LOHC as metal-free catalyst under mild conditions. This protocol could also dramatically expand the scope of convenient preparation of crystalline h-BN and its utilization in energy storage and conversion.

## Acknowledgements

The research was supported financially by the Division of Chemical Sciences, Geosciences, and Biosciences, Office of Basic Energy Sciences, US Department of Energy. J.F. was supported by the National Natural Science Foundation of China (No. 21436007, 21706228), the Zhejiang Provincial Natural Science Foundation of China (No. LR17B060002). The TEM imaging part of this research was completed at the Center for Nanophase Materials Sciences, which is a DOE Office of Science User Facility. This manuscript has been authored by UT-Battelle, LLC, under contract DE-AC05-00OR22725 with the US Department of Energy (DOE). The US government retains and the publisher, by accepting the article for publication, acknowledges that the US government retains a nonexclusive, paid-up, irrevocable, worldwide license to publish or reproduce the published form of this manuscript, or allow others to do so, for US government purposes. DOE will provide public access to these results of federally sponsored research in accordance with the DOE Public Access Plan (<http://energy.gov/downloads/doe-public-access-plan>).

**Keywords:** boron nitride • boron nitride nanosheet • crystallinity • magnesium • dehydrogenation

- [1] K. S. Novoselov, A. K. Geim, S. V. Morozov, D. Jiang, Y. Zhang, S. V. Dubonos, I. V. Grigorieva, A. A. Firsov, *Science* **2004**, 306, 666.
- [2] C. Tan, X. Cao, X.-J. Wu, Q. He, J. Yang, X. Zhang, J. Chen, W. Zhao, S. Han, G.-H. Nam, M. Sindoro, H. Zhang, *Chem. Rev.* **2017**, 117, 6225-6331.
- [3] X. Huang, X. Qi, F. Boey, H. Zhang, *Chem. Soc. Rev.* **2012**, 41, 666-686.
- [4] F. K. Kessler, Y. Zheng, D. Schwarz, C. Merschjann, W. Schnick, X. Wang, M. J. Bojdy, *Nat. Rev. Mater.* **2017**, 2, 17030.
- [5] A. Savateev, I. Ghosh, B. König, M. Antonietti, *Angew. Chem. Int. Ed.* **2018**, 57, 15936-15947.
- [6] Q. Weng, X. Wang, X. Wang, Y. Bando, D. Golberg, *Chem. Soc. Rev.* **2016**, 45, 3989-4012.
- [7] Q. Li, L. Chen, M. R. Gadinski, S. Zhang, G. Zhang, H. U. Li, E. Iagodkine, A. Haque, L.-Q. Chen, T. N. Jackson, Q. Wang, *Nature* **2015**, 523, 576.
- [8] W. Zhu, Z. Wu, G. S. Foo, X. Gao, M. Zhou, B. Liu, G. M. Veith, P. Wu, K. L. Browning, H. N. Lee, H. Li, S. Dai, H. Zhu, *Nat. Commun.* **2017**, 8, 15291.
- [9] P. Wu, S. Yang, W. Zhu, H. Li, Y. Chao, H. Zhu, H. Li, S. Dai, *Small* **2017**, 13, 1701857.
- [10] Y. Kubota, K. Watanabe, O. Tsuda, T. Taniguchi, *Science* **2007**, 317, 932-934.
- [11] J. T. Grant, C. A. Carrero, F. Goeltl, J. Venegas, P. Mueller, S. P. Burt, S. E. Specht, W. P. McDermott, A. Chieragato, I. Hermans, *Science* **2016**, 354, 1570-1573.

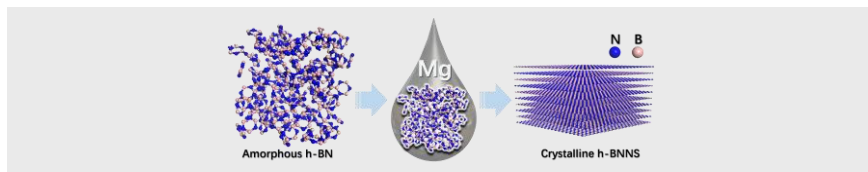
## COMMUNICATION

- [12] A. M. Love, B. Thomas, S. E. Specht, M. P. Hanrahan, J. M. Venegas, S. P. Burt, J. T. Grant, M. C. Cendejas, W. P. McDermott, A. J. Rossini, I. Hermans, *J. Am. Chem. Soc.* **2019**, *141*, 182-190.
- [13] S. Chen, R. Xu, J. Liu, X. Zou, L. Qiu, F. Kang, B. Liu, H.-M. Cheng, *Adv. Mater.* **2019**, *31*, 1804810.
- [14] A. Pakdel, Y. Bando, D. Golberg, *Chem. Soc. Rev.* **2014**, *43*, 934-959.
- [15] J. Yin, J. Li, Y. Hang, J. Yu, G. Tai, X. Li, Z. Zhang, W. Guo, *Small* **2016**, *12*, 2942-2968.
- [16] W. Zhu, X. Gao, Q. Li, H. Li, Y. Chao, M. Li, S. M. Mahurin, H. Li, H. Zhu, S. Dai, *Angew. Chem. Int. Ed.* **2016**, *55*, 10766-10770.
- [17] P. Wu, W. Zhu, Y. Chao, J. Zhang, P. Zhang, H. Zhu, C. Li, Z. Chen, H. Li, S. Dai, *Chem. Commun.* **2016**, *52*, 144-147.
- [18] M. Liu, K. Jiang, X. Ding, S. Wang, C. Zhang, J. Liu, Z. Zhan, G. Cheng, B. Li, H. Chen, S. Jin, B. Tan, *Adv. Mater.* **2019**, e1807865.
- [19] M. Zhao, Y. Huang, Y. Peng, Z. Huang, Q. Ma, H. Zhang, *Chem. Soc. Rev.* **2018**, *47*, 6267-6295.
- [20] C. S. Diercks, O. M. Yaghi, *Science* **2017**, *355*, eaal1585.
- [21] Z. Miao, G. Liu, Y. Cui, Z. Liu, J. Li, F. Han, Y. Liu, X. Sun, X. Gong, Y. Zhai, Y. Zhao, Y. Zeng, *Angew. Chem. Int. Ed.* **2019**, DOI: 10.1002/anie.201813999.
- [22] J. Xiong, W. Zhu, H. Li, W. Ding, Y. Chao, P. Wu, S. Xun, M. Zhang, H. Li, *Green Chem.* **2015**, *17*, 1647-1656.
- [23] A. Öya, S. Ötani, *Carbon* **1979**, *17*, 131-137.
- [24] A. Oberlin, *Carbon* **1984**, *22*, 521-541.
- [25] J. Peng, N. Chen, R. He, Z. Wang, S. Dai, X. Jin, *Angew. Chem. Int. Ed.* **2017**, *129*, 1777-1781.
- [26] L. Zhao, X. Zhao, L. T. Burke, J. C. Bennett, R. A. Dunlap, M. N. Obrovac, *ChemSusChem* **2017**, *10*, 3409-3418.
- [27] W. Lei, V. N. Mochalin, D. Liu, S. Qin, Y. Gogotsi, Y. Chen, *Nat. Commun.* **2015**, *6*, 8849.
- [28] L. H. Li, J. Cervenka, K. Watanabe, T. Taniguchi, Y. Chen, *ACS Nano* **2014**, *8*, 1457-1462.
- [29] C. Gervais, J. Maquet, F. Babonneau, C. Duriez, E. Framery, M. Vaultier, P. Florian, D. Massiot, *Chem. Mater.* **2001**, *13*, 1700-1707.
- [30] A. Öya, H. Marsh, *J. Mater. Sci.* **1982**, *17*, 309-322.
- [31] J. Yin, J. Li, Y. Hang, J. Yu, G. Tai, X. Li, Z. Zhang, W. Guo, *Small* **2016**, *12*, 2942-2968.
- [32] E. Gianotti, M. Taillades-Jacquín, J. Rozière, D. J. Jones, *ACS Catal.* **2018**, *8*, 4660-4680.
- [33] U. Eberle, M. Felderhoff, F. Schüth, *Angew. Chem. Int. Ed.* **2009**, *48*, 6608-6630.
- [34] P. Preuster, C. Papp, P. Wasserscheid, *Acc. Chem. Res.* **2017**, *50*, 74-85.
- [35] D. Teichmann, K. Stark, K. Müller, G. Zöttl, P. Wasserscheid, W. Arlt, *Energy Environ. Sci.* **2012**, *5*, 9044-9054.
- [36] M. C. Williams, J. P. Strakey, W. A. Surdoval, *J. Power Sources* **2005**, *143*, 191-196.
- [37] J. Tian, J. Tan, M. Xu, Z. Zhang, S. Wan, S. Wang, J. Lin, Y. Wang, *Sci. Adv.* **2019**, *5*, eaav8063.
- [38] Y. Wang, W.-C. Li, Y.-X. Zhou, R. Lu, A.-H. Lu, *Catal. Today* **2018**, <https://doi.org/10.1016/j.cattod.2018.1012.1028>.
- [39] F. Sotoodeh, K. J. Smith, *J. Catal.* **2011**, *279*, 36-47.

## COMMUNICATION

## Entry for the Table of Contents

## COMMUNICATION



Hao Chen, Zhenzhen Yang\*, Zihao Zhang, Zitao Chen, Miaofang Chi, Song Wang, Jie Fu\* and Sheng Dai\*

Page No. – Page No.

**A Strategy for Construction of a Nanoporous Highly Crystalline Hexagonal Boron Nitride from an Amorphous Precursor**

Highly crystalline nanoporous hexagonal boron nitride nanosheets (h-BNNS) were fabricated using amorphous h-BN precursors through a successive dissolution-precipitation/crystallization process in the presence of magnesium.